Ba0.77Ca0.23TiO3 (BCT) : a new photorefractive material to replace BaTiO3 in applications

Gérald Roosen, Sylvie Bernhardt, Philippe Delaye

$Ba_{0.77}Ca_{0,23}TiO_3$ (BCT) : a new photorefractive material to replace $BaTiO_3$ in applications

Gérald Roosen, Sylvie Bernhard, Philippe Delaye

Laboratoire Charles Fabry de l'Institut d'Optique, Unité Mixte de l'Institut d'Optique Théorique et Appliquée, du Centre National de la Recherche Scientifique et de l'Université Paris-Sud.

Centre Scientifique d'Orsay, Bat. 503, 91403 Orsay Cedex, France.

Corresponding author : Ph. Delaye, Tel : 33 1 69358750, Fax : 33 1 69358700,

Email : philippe.delaye@iota.u-psud.fr

The most popular photorefractive material $BaTiO_3$ suffers from a crippling defect when applications are considered : its phase transition around room temperature that can destroy its photorefractive characteristics, if not the crystal itself. Some years ago, University of Osnabrück [1], proposed and successfully grew $Ba_{0.77}Ca_{0.23}TiO_3$ an alloy derived from $BaTiO_3$, in which the phase transition was pushed away towards low temperature. The remaining question was then : does this new material keep the good photorefractive properties that made the success of $BaTiO_3$?

We will present here some theoretical and experimental results that allow us to answer this question and that show that despite some differences in the photorefractive properties between $BaTiO_3$ and BCT, the new crystal is an extremely promising materials for photorefractive applications, such as phase conjugation or dynamic holographic intracavity laser mode selection.

I. The photorefractive gain

The photorefractive performances of a photorefractive crystals are usually determined through a two beam coupling experiment and characterized by a photorefractive gain that writes as [2, 3]:

$$\Gamma = \frac{2\pi}{\lambda_0} n^3 r^{eff} E_{SC}(k_r, I)(\hat{e}_S.\hat{e}_P) \qquad (1)$$

where λ_o is the wavelength in vacuum, n the mean refractive index and $(\hat{e}_s.\hat{e}_p)$ is the scalar product of the polarization vectors of the beams. r^{eff} the effective electro-optic coefficient depends on the crystal orientation and on the polarization of the beams and $E_{SC}(k_r, I)$ is the space charge field that

depends on the grating spacing k_r and on I the incident illumination on the crystal. In a new crystal such as BCT both quantities are a priori unknown and will have to be determined through photorefractive experiments.

The main idea of this characterization is linked to the nature of the two quantities we want to determine. First, the effective electro-optic coefficient will be linked to the crystalline structure of the material, it will be dopant independent. Crystals grown with different doping conditions (as soon as they present photorefractive effect) will have similar orientation dependence of the gain. Second, for a given orientation, the grating spacing and intensity dependence of the photorefractive gain will be only dependent on the deep defects responsible for the photorefractive effect. Both problems are thus separable and, in a first approximation, we can deduce some information on the charge transport model valid for BCT without knowing the exact value of the electo-optic coefficients, and inversely, we can measure the effective electro-optic coefficient without knowing the nature of the defect involved in the space charge field. This nevertheless requires to perform some specific experiments that will be presented in the following.

II. Two beam coupling energy transfer measurement

The basic and mostly used experiment for photorefractive crystal characterization is the two beam coupling energy transfer gain. The two beam coupling experimental set-up is presented in Figure 1. The beam from a laser is divided in two by a glass plate. The powerful transmitted beam is called the pump beam, whereas the weak reflected beam is called the signal beam. Both beams are sent on the photorefractive crystal where they interfere and create an index grating on which they diffract. The $\pi/2$ phase shift between the index grating and the illumination pattern, characteristic of the photorefractive effect leads to an energy transfer between the two beams (Figure 2). From the steady state intensities of the transmitted weak signal beam without (I_S) and with (I_{SP}) illumination by the pump beam, we calculate the photorefractive gain Γ thanks to the relation (using ℓ the length of the crystal) [2]:

$$\Gamma = \frac{1}{\ell} \ln \frac{I_{SP}}{I_S} \qquad (2)$$

The parameters of the experiment (grating spacing, illumination, crystal orientation, polarization,…) are changed and the variation of the gain as a function of these parameters is measured.

III. Orientation dependence of the photorefractive gain : determination of the electro-optic coefficients

Two symmetrical beams forming an angle 2θ inside the material enter symmetrically the crystal, which then turns round the normal to the crystal (y-axis) (Figure 3) [4]. The angle of rotation is α. We start with α=0° and then the c-axis is in the (x,y) plane. β is defined as the angle between the c-axis and its projection on the (z-x)-plan. θ and β are defined inside the crystal. From the energy transfer, we measure the photorefractive gain as a function of the rotation angle α. To always enter the crystal with eigen-polarizations (ordinary or extraordinary), the polarizations are rotated by the same angle α.

When a small angle between the beams is used, the space charge field is usually dominated by the diffusion field and the photorefractive gain writes as :

$$\Gamma \approx \frac{2\pi}{\lambda_0} n^3 r^{eff} \frac{k_B T}{e} k_r \qquad (3)$$

The only orientation dependent contribution is the effective electro-optic coefficient one. In photorefractive crystal such as $BaTiO_3$ or $KnbO_3$ this dependence can be rather complex due to the influence of the indirect electro-optic effect (created by the deformation of the crystal induced by the piezoelectric effect), and depart from the usual sinusoidal variation of the gain with the rotation angle α [4].

In the case of the BCT [5] the same kind of non sinusoidal variation is observed but to a smaller extent than in $BaTiO_3$ (Figure 4). Measurement were performed in two crystals of BCT doped with different concentration of rhodium (100ppm of Rh added in the melt in B69 and 1000ppm of Rh in B76). The crystals were grown at the university of Osnabrück and polished at FEE GmbH. The presented data corresponds to measurements performed at 514nm [5], but similar results were obtained at 850nm [6]. The fact that the curves present the same shape in the two sample confirms that the observed effect is essentially independent of the doping concentration. Nevertheless a little difference in the amplitude of the two curves shows that a sample dependent reduction factor exists. Its origin is still not identified. It can be due to the presence of an electron-hole competition [7] that can reduce the amplitude of the space charge field, or the presence of a secondary defect [8] that cause the presence of an intensity dependent gain reduction coefficient (the gain is nevertheless intensity independent around the measurement intensity). The third possibility can be due to an imperfect poling of the sample [9] that can cause a reduction of the effective interaction length of the crystal.

The shape of the curves gives some information on important parameters of the BCT crystal (piezo-electric, elastic and elasto-optic coefficients). This analysis is complex due to the large number of coefficients involved in the modelization (at least 21). To reduce this number of coefficients we use a well known characteristics of perovskites crystals of the $BaTiO_3$ family, that is that the cubic phase parameters (electrostriction and Kerr electro-optic coefficients) are transformed into the parameters of the room temperature quadratic phase (piezoelectric or Pockels electro-optic coefficients) by the spontaneous polarization that appears in the phase transition. A simple model [10] allows to calculate all the quadratic phase parameters using the cubic phase parameters and some known coefficients of the quadratic phase such as the unclamped dielectric constant or the birefringence of the crystal. This model allows to reduce the number of free parameters from 21 to less than 16. For these unknown parameters, we use, as an initial set of parameters, the coefficient found in the literature for $BaTiO_3$, using the fact that BCT is an alloy derived from $BaTiO_3$ that stays close to it in its structure. All the quadratic phase coefficients of BCT can thus be calculated and the rotation dependence gain can be simulated and compared to experimental curves. The obtained curves have a similar shape but a different amplitude [5]. The difference in amplitude was as above entirely attributed to the sample dependent reduction coefficient of unknown origin (with a value of 0.7 and 0.5 in the tested samples), and the theoretical curves were finely adjusted slightly changing only two parameters (the Kerr coefficients g_{11}^S and g_{12}^S that were changed by less than 30%).

Besides these curves some other measurements were performed in some other samples with different orientations, such as a 45°-cut sample. In this sample the measured curves compares exactly to the calculated curves using the same cubic phase coefficients than in the other sample and with a reduction coefficient of about 0.5 [5]. In the 0° cut B69 sample we also make a measurement as a function of the angle β between the c-axis and the grating vector around $\beta=\pi/2$ (Figure 5). The slope of the linear dependence is directly linked to the r_{42} coefficient and allows the determination of the g_{44}^S Kerr coefficient, taking into account the reduction coefficient previously determined in the used sample[5, 10].

The result of this study is an evaluation of the complete set of parameters of the BCT crystal, both in the cubic phase (Table 1) and in the quadratic phase (Table 2) [5]. The presented data are just a set of parameters that is compatible with the experimental data we obtained. This set is certainly not unique due to the limited number of measured data and the great number of parameters. It was obtained with some approximations (for exemple the whole difference in amplitude is attributed to the reduction coefficient) and more over some parameters have only little influence on the calculated curves (such as p_{66}^p and s_{66}^p). It is also certainly not far from the actual

one as some of the determined coefficient (such as r_{13}^T and r_{33}^T) are close to the value found in the literature from independent measurement (36pm.V^{-1} and 140pm.V^{-1} respectively [11]).

All these data are important for the evaluation of the cut of the BCT crystal that will allow the best performances. With the above coefficients it can be calculated that the highest photorefractive gain is obtained in a 45° cut sample, with gain as high as 80cm^{-1} expected at 514nm [5].

IV. Determination of the charge transfer model

The second important characteristics of a photorefractive material is the charge transport model that is responsible for the creation of the space charge field. This charge transport model depends on the deep defects inserted in the material through doping or eventually through post growth treatment. In the case of $BaTiO_3$, one very popular doping is the rhodium doping that is responsible for the infrared sensitivity of the material [12,13]. The question of the infrared sensitivity of BCT soon arises after the successful growth of that crystal. Several rhodium doped BCT crystals were grown by university of Osnabrück and their photorefractive characteristics measured at 850nm [14, 15]. The rhodium concentration varies from 220ppm to 2000ppm of rhodium added in the melt, in addition an undoped sample and a 140ppm iron doped sample were studied. We analyzed the photorefractive behaviour of these different samples in a two beam coupling set-up at the wavelength of 850nm.

The first experiment to perform when studying a photorefractive material is to measure the absorption spectra. The spectra of the different samples (Figure 6) show a strong absorption band (around 600-700nm), similar to the one observed in Rhodium doped $BaTiO_3$ [12] that increases proportionally to the rhodium concentration. The observation of such an absorption band is a condition to obtain a good sensitivity in the infrared as it shows that rhodium is incorporated in the BCT matrix and that it absorbs light to create holes. These measurements also reveal the presence of an absorption structure that superimposes to the rhodium structure in the low wavelength range of the spectrum in the low doped samples. This structure also present in the undoped and in the iron doped sample was attributed to the additional presence of iron in all the samples [14]. This constatation is of importance if we remember that the iron is known to be responsible for the photorefractive sensitivity of undoped $BaTiO_3$.

Then we performed two beam coupling measurements as a function of the grating spacing and the incident illumination (Figure 7 and 8). The measurement was performed at a fixed grating orientation (grating spacing along the c-axis) and with ordinary polarized beams (to prevent the problems of beam fanning and oscillation encountered with the high gain observed with

extraordinary polarization) issued from a 100mW DBR laser diode emitting at 850nm [14]. In this configuration the electro-optic coefficient is constant and equals $r_{22}^{eff} = r_{13}^{S} + p_{13}^{E} e_{33} / c_{33}^{E}$ [10].

The experimental data were adjusted with the classic theoretical expression that gives the variation of the space charge field with grating wave number k_r and incident illumination [2] :

$$E_{SC}(k_r, I) = \frac{k_B T}{e} \eta(I) \frac{k_r}{1 + \frac{k_r^2}{k_0^2(I)}} \tag{4}$$

$\eta(I)$ expresses the saturation of the gain with intensity, which is related to the ratio between photoconductivity and dark conductivity, and writes as :

$$\eta(I) = \frac{1}{1 + \frac{I_{sat}}{I}} \tag{5}$$

In Eq. (4), the second term depending on intensity is the Debye screening wave vector k_o, which depends on the effective trap density as :

$$k_0^2(I) = \frac{e^2 N_{eff}(I)}{k_B T \varepsilon_0 \varepsilon^{eff}} \tag{6}$$

where ε^{eff} is the effective dielectric constant [10].

These expression were initially established in the framework of a one defect – one carrier model [2], but it can be shown that they stay valid eventually with some minor arrangement with more complex charge transport models [7, 8, 16]. Using these expressions we determine the different experimental parameters that governs the efficiency of the photorefractive effect, and that are summarized in Table 3. We see that the saturation intensity decreases with the doping concentration where as strong photorefractive gain is observed in all the samples with similar values of the effective electro-optic coefficient as expected but also more surprisingly similar values of the effective trap density. These results seems to indicate at first look that the photorefractive effect is not linked to the rhodium doping as photorefractive effect is observed even in the undoped of the iron doped sample.

To solve the apparent contradiction between these different results and after having eliminated the different possible model [15], we arrive to the conclusion that rhodium is really the defect involved in the photorefractive effect (with its three state of charge as in $BaTiO_3$) but that another defect in large concentration is also present (Figure 9) and is responsible for the photorefractive effect for low concentrations or in the absence of rhodium. This secondary defect is attributed to the iron doping, even if the knowledge of its exact nature is not essential to the conclusions derived here.

Using this new charge transport model [14], we were able to simulate the grating wavenumber and illumination variation of the photorefractive gain. To determine the parameters of the iron level we use the undoped crystal. In that case (no rhodium) the model simplifies and becomes analytical, what allow to determine the concentrations of the iron level and of the compensating levels (N_d - N_a), which concentrations were supposed to be the same in all the other samples. For the rhodium level parameters we use as initial value the parameters of $BaTiO_3$:Rh, and change the parameters until a good accordance between theoretical simulation and experimental data. The set of parameters that allows to obtain the theoretical curves presented in Figures 7 and 8 is given in Table 4.

Despite its low photoionisation cross-section, the influence of iron is very important due to its very large concentration. This large concentration (compared to what is usually observed in $BaTiO_3$) might be due to the growth temperature, which is 200°C higher for BCT than for $BaTiO_3$, and that may favor the incorporation of iron in the crystal. This large amount of iron that is found in BCT crystals is in good accordance with EPR measurements performed at the University of Osnabrück [17]. Concerning the photorefractive properties this large concentration of iron is mainly prejudiciable as it increases in an important manner the saturation intensity, which means that very high illumination is necessary to saturate the photorefractive gain.

The influence of iron is observable until high concentration of rhodium. Simulations shows that it is only above 2000ppm added in the melt that rhodium becomes preponderant in the photorefractive properties. To verify this point two new samples with higher doping (4000ppm and 10000ppm added in the melt) has been grown by university of Osnabrück, and characterized in a two beam coupling experiment at 850nm. We first observe that the absorption continue to increase in proportion of the doping concentration (Figure 10) showing that rhodium continues to incorporate in the BCT matrix even at this very high doping levels. Concerning the photorefractive performances we measure the photorefractive gain as a function of the grating spacing and as a function of illumination. Concerning illumination dependence, the large absorption of the crystal at the used wavelength prevents a clear interpretation of the data. The illumination varies a lot during the propagation of the beams and thus can not be considered as constant during propagation in the crystal as supposed in the model. Nevertheless the obtained data are coherent with the theoretical simulations, the important point being that saturation of the gain is easily obtained in the new crystals. For the grating spacing dependence (Figure 11), we observe a strong increase of the gain measured in a counterpropagating geometry (i.e. large value of the grating wavenumber k_r). This corresponds to an increase of the effective trap density due to the higher rhodium doping. At low rhodium doping (i.e. below 2000ppm) the iron concentration is the highest and the effective trap density is governed by the iron concentration and is thus independent of rhodium concentration.

Above 2000ppm rhodium becomes preponderant and the effective trap density increases with rhodium doping.

V. Conclusion

We present here an extensive study of the photorefractive properties of rhodium doped BCT crystals. The main results of this study are to show that the photorefractive properties of BCT are very close to the ones of $BaTiO_3$. High gain is obtained due to high values of the electro-optic coefficient. Despite its smaller value compared to $BaTiO_3$ the r_{42} coefficient stays sufficiently large to allow the observation of large photorefractive energy coupling gain in BCT crystals with optimized cut (45°-cut sample). Like $BaTiO_3$, BCT presents infrared sensitivity until 850nm and even 1.06µm (new results not presented here). The charge transport model is more complex than in $BaTiO_3$ due to the presence of a large quantity of iron in BCT. But here too the performances are sufficient for most applications of this crystal. These measurements show that BCT is a good alternative to $BaTiO_3$, as soon as industrial applications are considered and when the phase transition of $BaTiO_3$ can be a major drawback. Future study of this new crystal, should go in the direction of the increase of knowledge on the properties of this crystal, photorefractive characteristics, but also mechanical, electrical or optical properties, in order to reach a level of knowledge similar to $BaTiO_3$. On the photorefractive point of view, some other typical dopant used in $BaTiO_3$ (such as cobalt or cerium) should be tested in BCT, whereas the comprehension of the insertion and of the role of iron should be improved, in order to eliminate it from the growth and improve the performances of BCT.

Acknowledgment :

We gratefully acknowledge contributions from H. Veenhuis, R. Pankrath and O.F. Schirmer (University of Osnabrück), D. Rytz (FEE GmbH) and L. Mize (LCFIO, National Science Foundation International REU Program)

References

[1] Ch.Kuper, R.Pankrath, H.Hesse. "Growth and dielectric properties of congruently melting $Ba_{1-x}Ca_xTiO_3$ crystals", Appl. Phys. A. **65**, 301 (1997).

[2] N.V. Kukhtarev, V.B. Markov, S.G. Odulov, M.S. Soskin, V.L. Vinetskii, "Holographic storage in electrooptic crystals I. Steady state", Ferroelectrics **22**, 949 (1979) and Ferroelectrics **22**, 961 (1979).

[3] G. Montemezzani, "Optimization of photorefractive two-wave mixing by accounting for material anisotropies : $KNbO_3$ and $BaTiO_3$", Phys.Rev. **A 62**, 053803 (2000).

[4] M. Zgonik, K. Nakagawa, P. Günter, "Electro-optic and dielectric properties of photorefractive $BaTiO_3$ and $KNbO_3$", J. Opt. Soc. Am. B **12**, 1416 (1995).

[5] S.Bernhardt, L. Mize, P. Delaye, R. Pankrath, O.F. Schirmer, G. Roosen, "Orientation dependence of photorefractive gain in BCT : determination of electrooptic coefficients." OSA Trends in Optics and Photonics, Advances in photorefractive Materials, Effects, and Devices, **62** 504 (2001).

[6] S. Bernhardt, "Gyromètre à fibre à double conjugaison de phase : étude d'un nouveau matériau photoréfractif, réalisation d'un démonstrateur" Thèse de doctorat de l'Université Paris Sud (Orsay) (2001).

[7] F.P. Strohkendl, J.M.C. Jonathan, R.W. Hellwarth, "Hole-electron competition in photorefractive gratings", Opt. Lett. **11**, 312 (1986).

[8] P. Tayebati, C. Mahgerefteh, "Theory of the photorefractive effect for $Bi_{12}SiO_{20}$ and $BaTiO_3$ with shallow traps", J. Opt. Soc. Am. **B 8**, 1053 (1991).

[9] M.B. Klein, G.C. Valley, "Beam coupling in $BaTiO_3$ at 442 nm." J. Appl. Phys. **57**, 4901 (1985).

[10] S. Bernhardt, P. Delaye, H. Veenhuis, D. Rytz, G. Roosen, "Photorefractive two-beam coupling characterization of a barium-calcium titanate crystal", Appl. Phys. B **70**, 789 (2000).

[11] C.Kuper, K. Buse, U. van Stevendaal, M. Weber, T. Leidlo, H. Hesse, E.Krätzig, "Electrooptic and photorefractive properties of ferroelectric barium-calcium titanate crystals" Ferroelectics **208-209**, 213 (1998).

[12] H.Kröse, R.Scharfschwerdt, O.F.Schirmer, H.Hesse, “Light-induced charge transport in $BaTiO_3$ via three charge states of rhodium”, Appl. Phys. B **61**, 1 (1995).

[13] N.Huot, J.M.C.Jonathan, G.Roosen, “Validity of the three charge state model in photorefractive $BaTiO_3$:Rh at 1.06 μm in the cw regime”, Appl. Phys. B. **65**, 486 (1997).

[14] S. Bernhardt, H. Veenhuis, Ph. Delaye, R. Pankrath, G. Roosen. "Effect of rhodium doping on the photorefractive properties of BCT crystals at 850nm". Applied Physics **B72**, 667 (2001). (Errata) Applied Physics **B74**, 287 (2002).

[15] S. Bernhardt, H. Veenhuis, Ph. Delaye, G.Roosen. "Characterization of rhodium and iron doped $Ba_{0,77}Ca_{0,23}TiO_3$ crystals at 850nm", Optical Materials **18**, 13 (2001).

[16] Ph.Delaye, L.A. de Montmorillon, I.Biaggio, J.C.Launay, G.Roosen, "Wavelength dependent effective trap density in CdTe : evidence for the presence of two photorefractive species", Optics Commun. **134**, 580 (1997).

[17] O.F.Schirmer, private communication.

Figure Captions

Figure 1 : Two-beam coupling set-up.

Figure 2 : Typical energy transfer signal.

Figure 3 : Scheme of the orientation of the crystal for the rotation measurement.

Figure 4 : Experimental photorefractive gain as a function of the angle α for ordinary (A) and extraordinary (B) polarizations for the crystal B69 and B76. The lines represents the best fits to the experimental curves (see the following of the text).

Figure 5 : Gain as a function of β around $\pi/2$ (comparison with simulations). The insert shows the used configuration.

Figure 6 : Absorption spectra of BCT as a function of rhodium doping.

Figure 7 : Normalized photorefractive gain (normalization to the saturation value given by the adjustment) versus incident illumination. The points corresponds to experimental data and lines corresponds to the calculation using the three levels charge transport model. Measurements are obtained at a small value of the grating wavenumber.

Figure 8 : Photorefractive gain versus grating wavenumber. The points corresponds to experimental data and lines corresponds to the calculation using the three levels charge transport model (and the adjusted value of the effective electro-optic coefficient). Measurements are performed at maximum illumination with ordinary polarized beams.

Figure 9 : Schematic representation of the energy levels in a BCT:Rh crystal with iron as an additional impurity center.

Figure 10 : Absorption spectra of 4000ppm and 10000ppm rhodium BCT cristals.

Figure 11 : Photorefractive gain as a function of the grating wavenumber for ordinary polarization for BCT:Rh sample with doping until 10000ppm. The points corresponds to experimental data and the lines to the theoretical simulation with new charge transport model.

Table Caption

Table 1 : Final set of parameters determined for BCT in the cubic phase.

Table 2 : Final quadratic phase parameters deduced from the cubic phase parameters of table 1.

Tableau 3 : Values of the saturation intensity, of the effective trap density and of the effective electro-optic coefficient for BCT:Rh crystals from 0 to 2000ppm.

Table 4 : Parameters of rhodium and iron used in the calculation of the photorefractive gain in BCT:Rh.

Clamped Kerr coefficients (10^{-2} $m^4.C^{-2}$)		Electrostriction coefficients ($m^4.C^{-2}$)	
g_{11}^S	**11**	Q_{11}	0.09
g_{12}^S	**3.5**	Q_{12}	-0.04
g_{44}^S	**13.5**	Q_{44}	0.06
Elasto-optic coefficients at constant polarization		Elastic constants at constant polarization (10^{-12} $m^2.N^{-1}$)	
p_{11}^P	0.37	s_{11}^P	8.7
p_{12}^P	0.11	s_{12}^P	-3.35
p_{66}^P	-0.30	s_{66}^P	8.9
Index and birefringence		Unclamped dielectric constant	
n	2.46	ε_{11}^T	1120
Δn	0.05	ε_{33}^T	240

Table 1

Clamped dielectric constants		Spontaneous polarization ($C.m^{-2}$)	
ε_{11}^{S}	824	P_S	0.30
ε_{33}^{S}	140	Elasto-optic coefficients at constant field	
Elastic stiffness at constant field ($10^{10}N.m^{-2}$)		p_{11}^{E}	0.34
c_{11}^{E}	22	p_{12}^{E}	0.08
c_{33}^{E}	18.7	p_{13}^{E}	0.25
c_{12}^{E}	13.7	p_{31}^{E}	0.02
c_{13}^{E}	14.6	p_{33}^{E}	0.80
c_{44}^{E}	8.3	p_{44}^{E}	0.89
c_{66}^{E}	11.2	p_{66}^{E}	-0.30
Piezoelectric coefficients ($pm.V^{-1}$)		Piezoelectric coefficients ($C.m^{-2}$)	
d_{31}	-51	e_{31}	-1.42
d_{33}	114	e_{33}	6.52
d_{24}	178	e_{24}	14.7
Unclamped electrooptic coefficients ($pm.V^{-1}$)		Clamped electrooptic coefficients ($pm.V^{-1}$)	
r_{13}^{T}	33	r_{13}^{S}	26
r_{33}^{T}	170	r_{33}^{S}	81
r_{42}^{T}	453	r_{42}^{S}	295

Table 2

Cristal	I_{sat} (mW.cm^{-2})	N_{eff} ($\times 10^{22}$ m^{-3})	r_{22}^{eff} (pm.V^{-1})
BCT:Fe 140 ppm	1300	5,4	15
BCT non dopé	360	6,2	11,6
BCT:Rh 200 ppm	190	4,9	12,8
BCT:Rh 370 ppm	170	6,1	13
BCT:Rh 600 ppm	110	7,1	12,8
BCT:Rh 1000 ppm	100	5,3	13,6
BCT:Rh 2000 ppm	90	7,2	15,3

Table 3

Parameters	Adjusted value for BCT:Rh
Photoionization cross section of Rh^{5+} : S^{+} (m^2)	9×10^{-21}
Photoionization cross section of Rh^{4+} : S^{-} (m^2)	0.4×10^{-21}
Photoionization cross section of Fe^{4+} : S_F (m^2)	0.001×10^{-21}
Recombination rate on Rh^{4+} (m^3/s) : γ_+	2.92×10^{-14}
Recombination rate on Rh^{3+} (m^3/s) : γ_-	$15*\gamma_+$
Recombination rate on Fe^{3+} (m^3/s) : γ_F	γ_+
Thermal emission rate of Rh^{5+} (s^{-1}) : β^+	2.3
Thermal emission rate of Rh^{4+} (s^{-1}) : β^-	0.0001
Thermal emission rate of Fe^{4+} (s^{-1}) : β_F	0.000125
Total Iron concentration (m^{-3}) : N_F	64×10^{23}
Compensation density (m^{-3}) : $N_{DA} = N_d - N_a$	0.82×10^{23}
Total concentration of rhodium for a 1000 ppm doped sample(m^{-3}) : N_T	3.3×10^{23}

Table 4

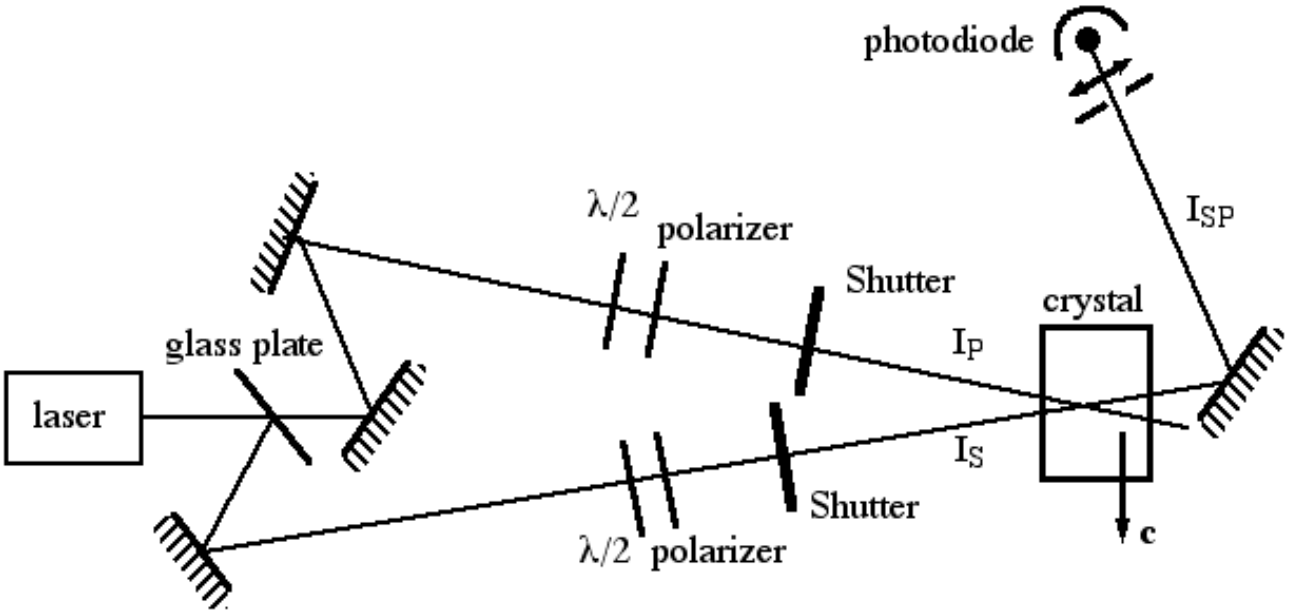

Figure 1 : Roosen et al

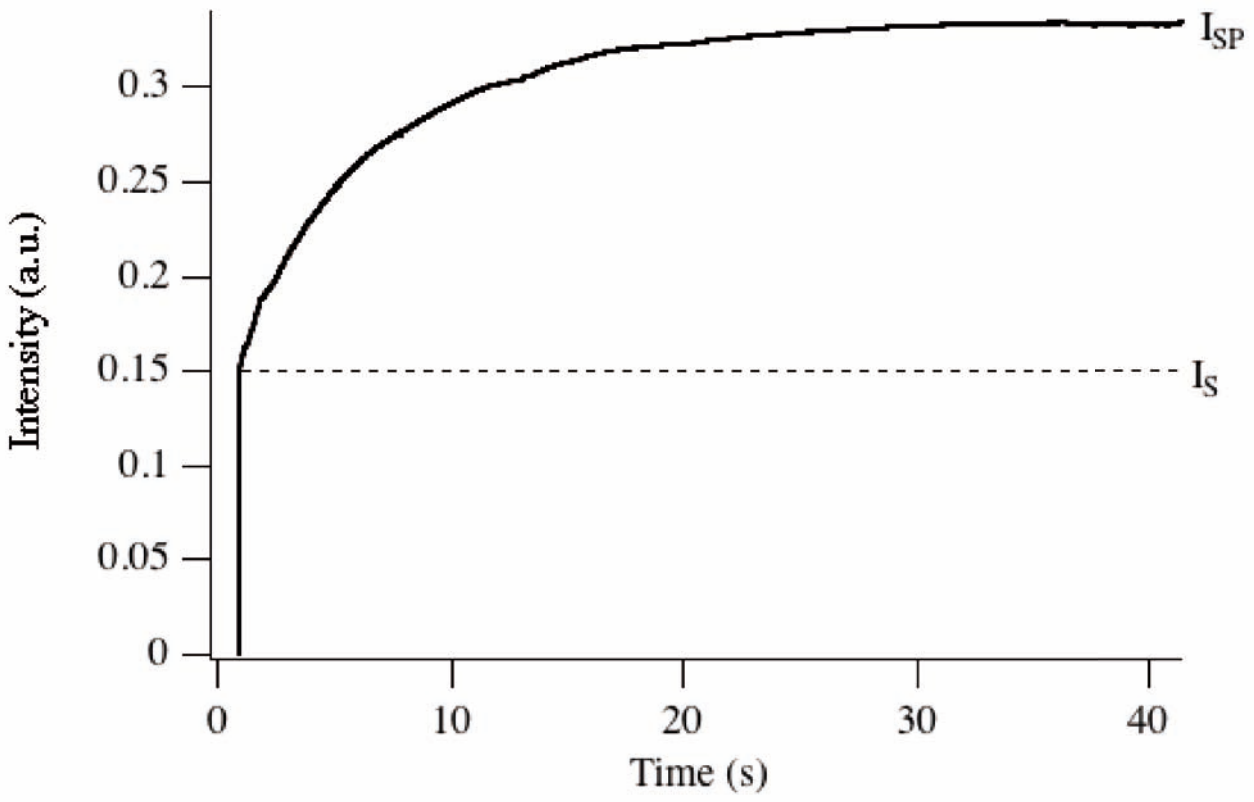

Figure 2 : Roosen et al.

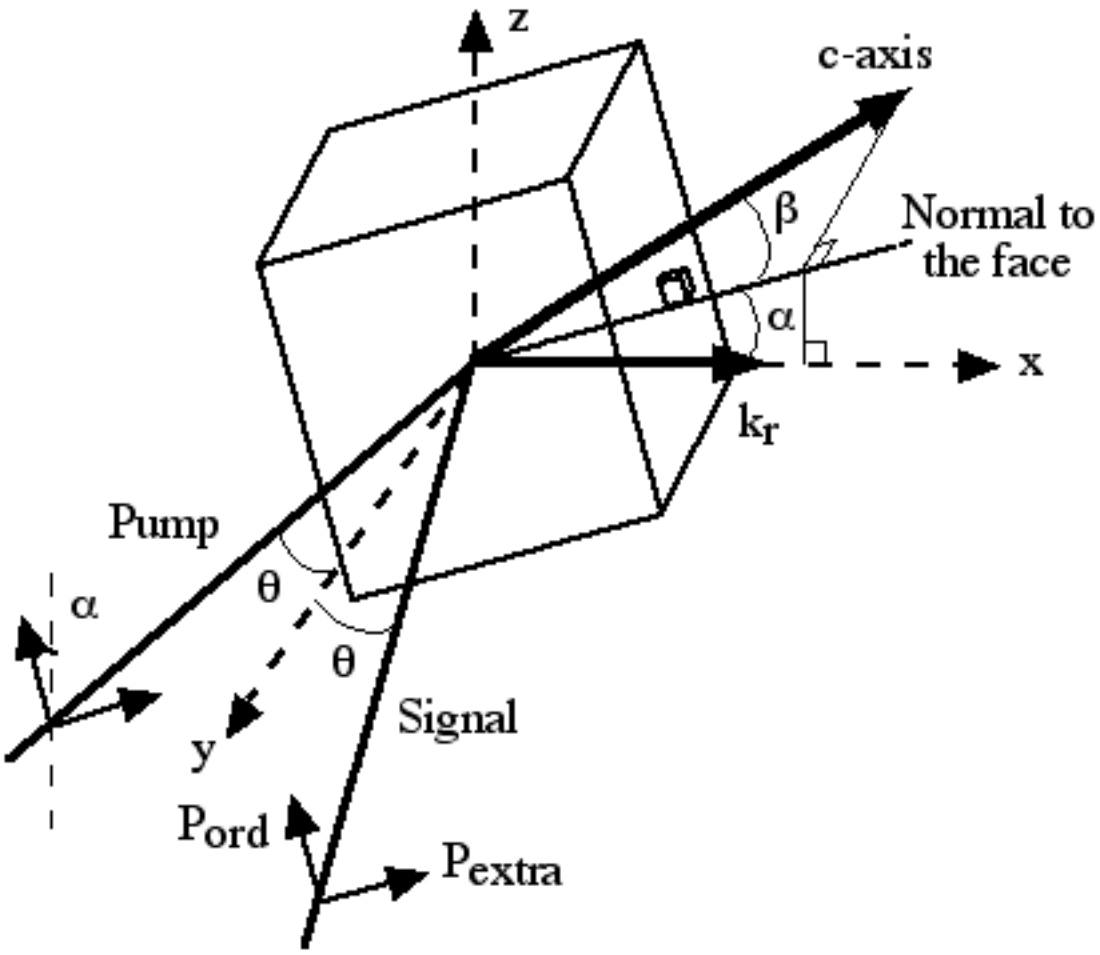

Figure 3 : Roosen et al

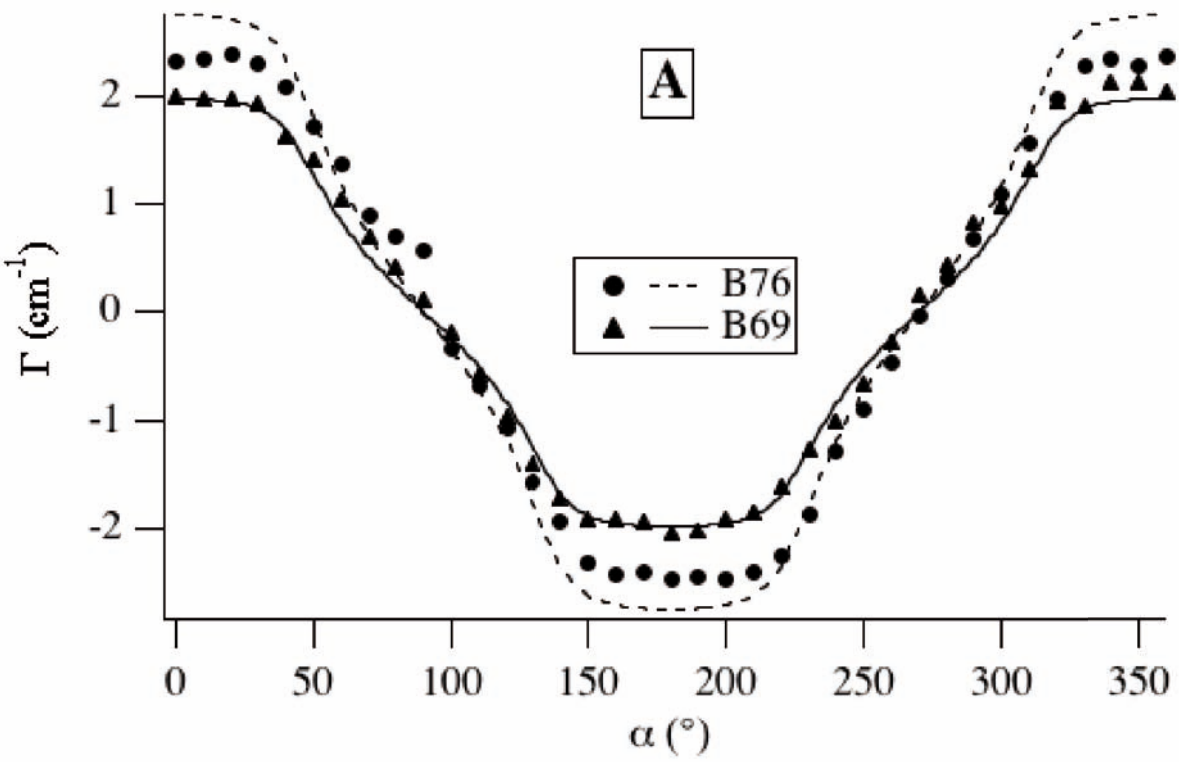

Figure 4a : Roosen et al.

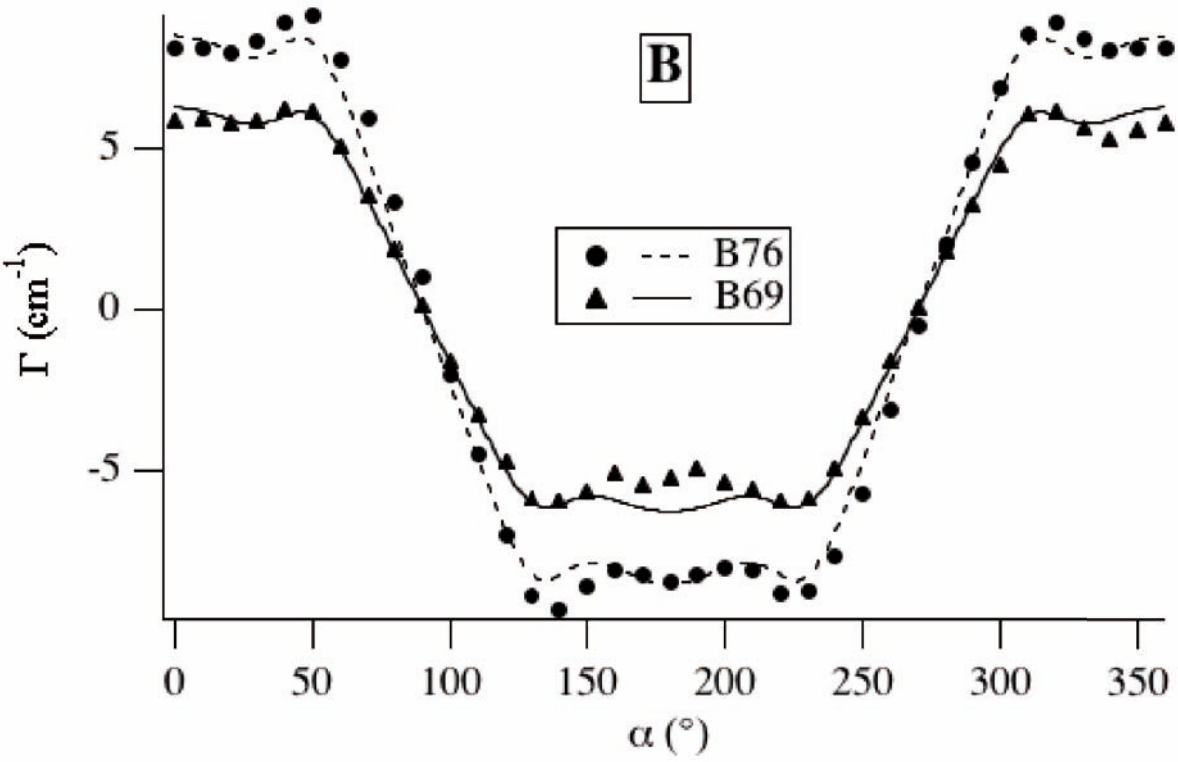

Figure 4b : Roosen et al.

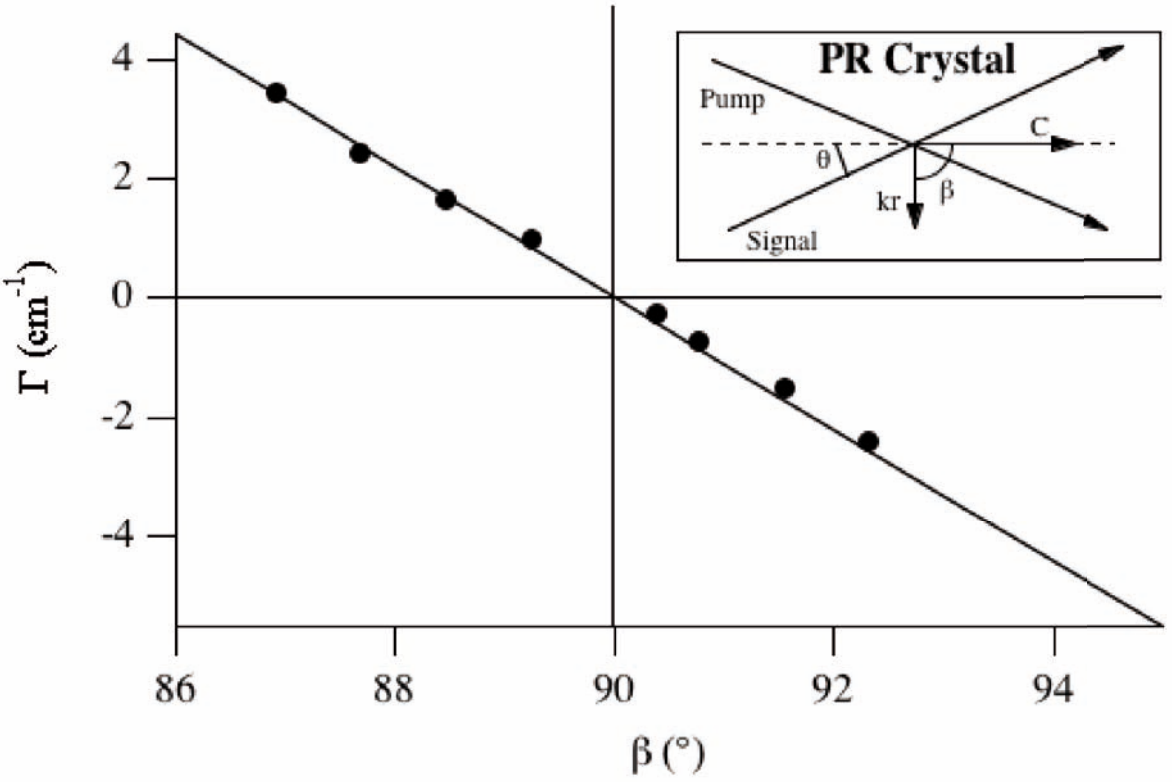

Figure 5 : Roosen et al.

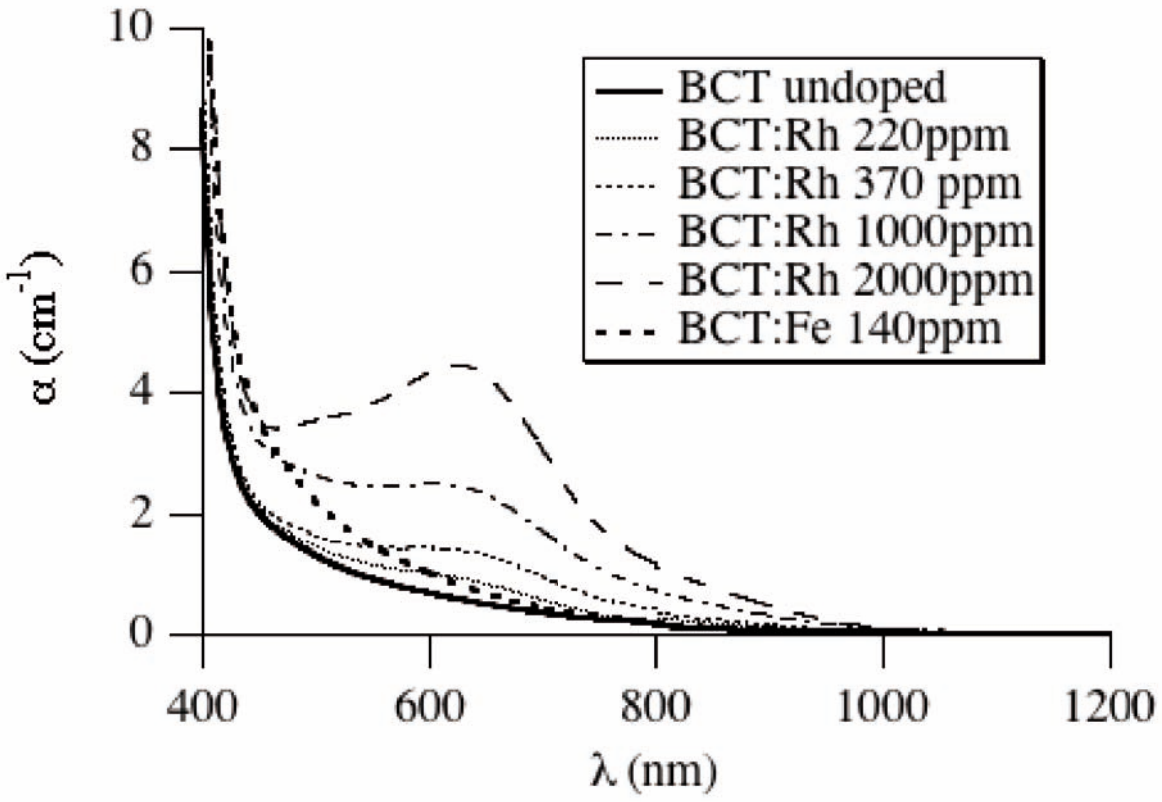

Figure 6 : Roosen et al.

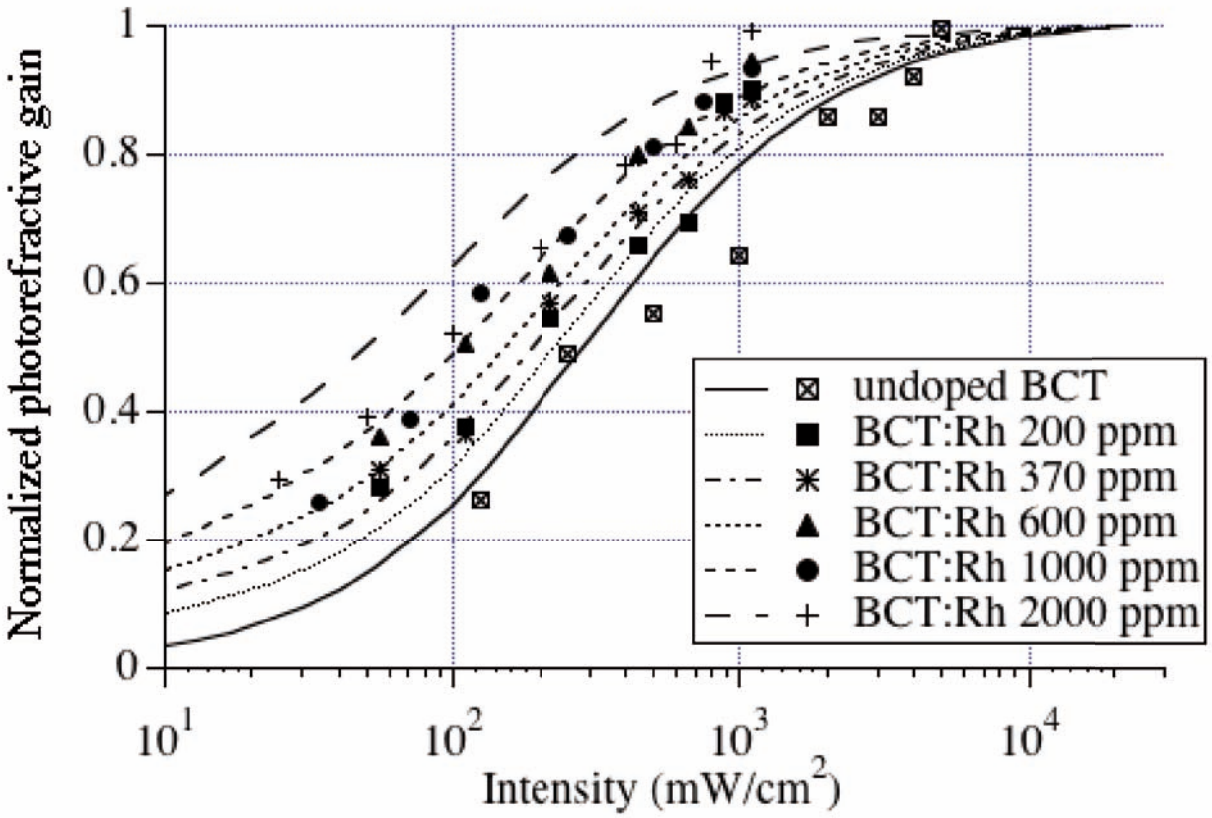

Figure 7 : Roosen et al.

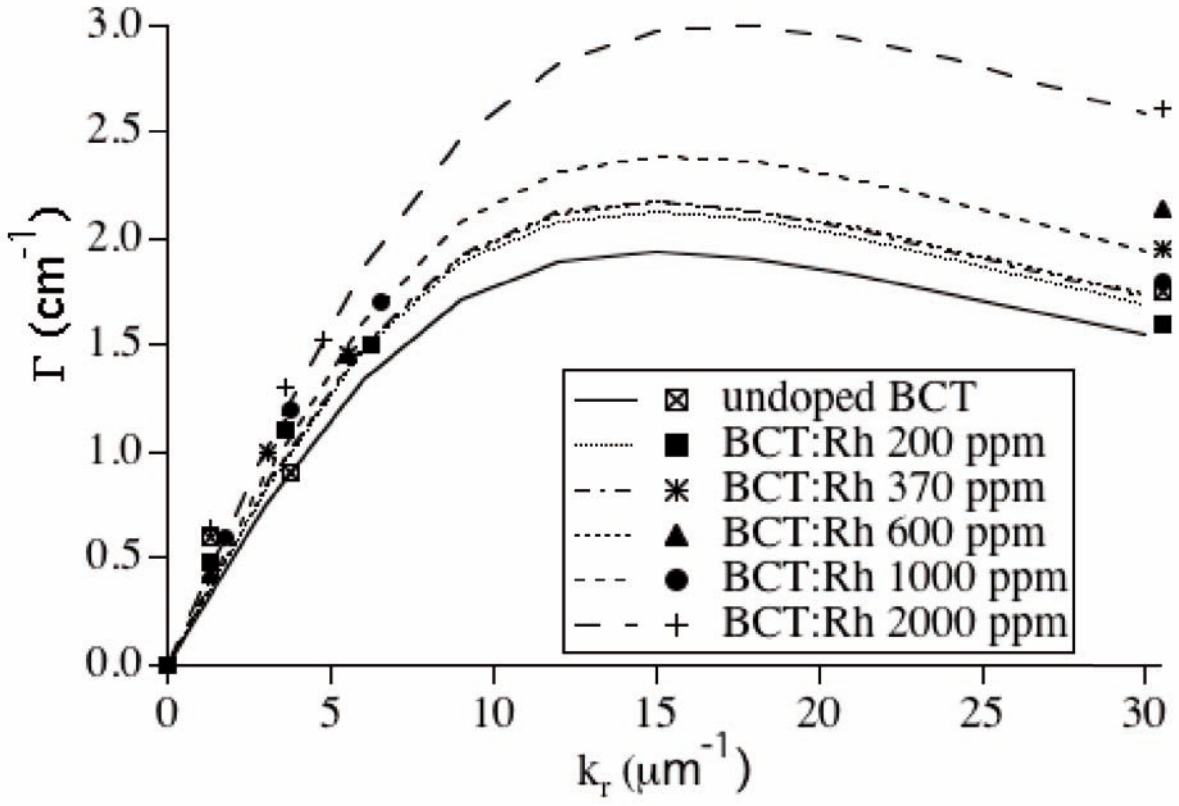

Figure 8 : Roosen et al.

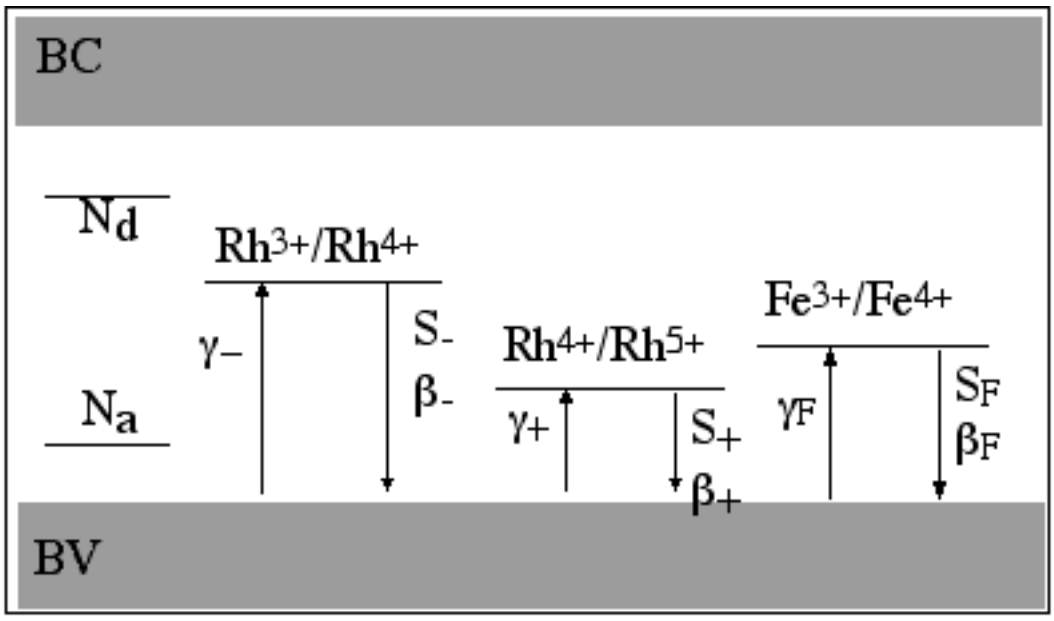

Figure 9 : Roosen et al.

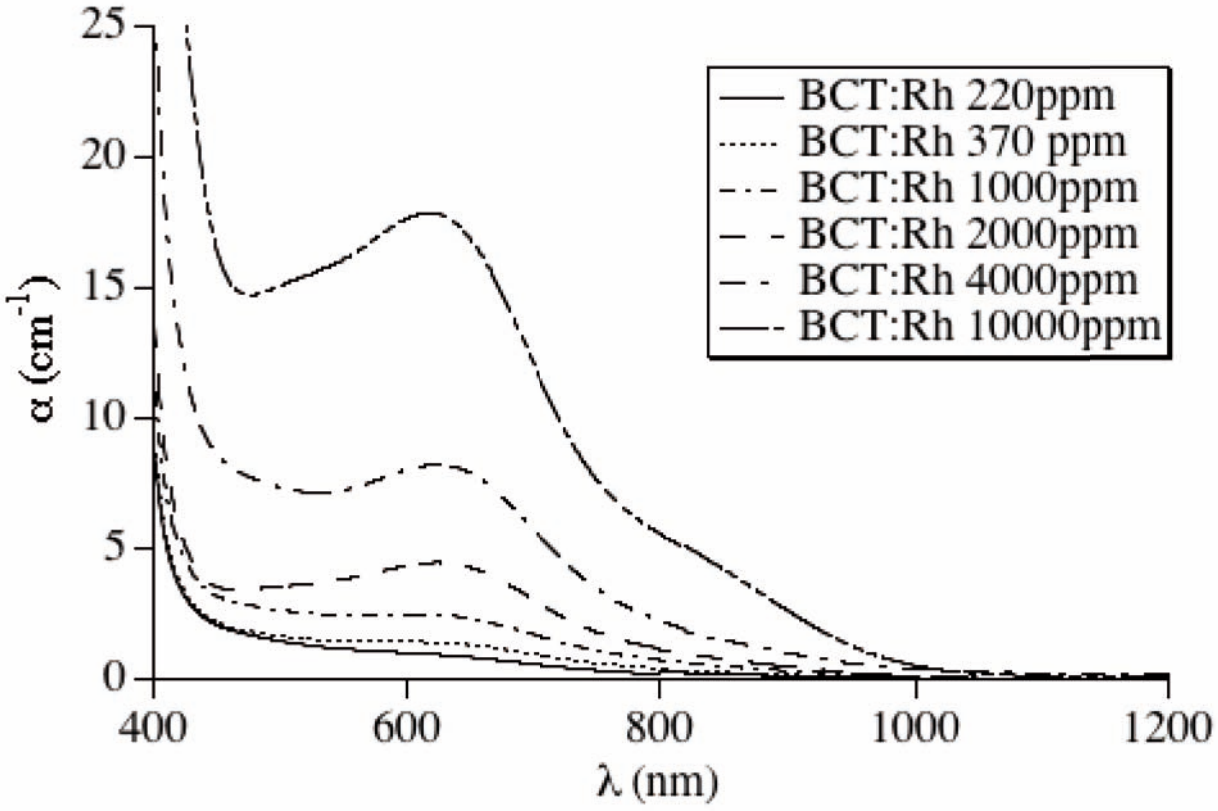

Figure 10 : Roosen et al.

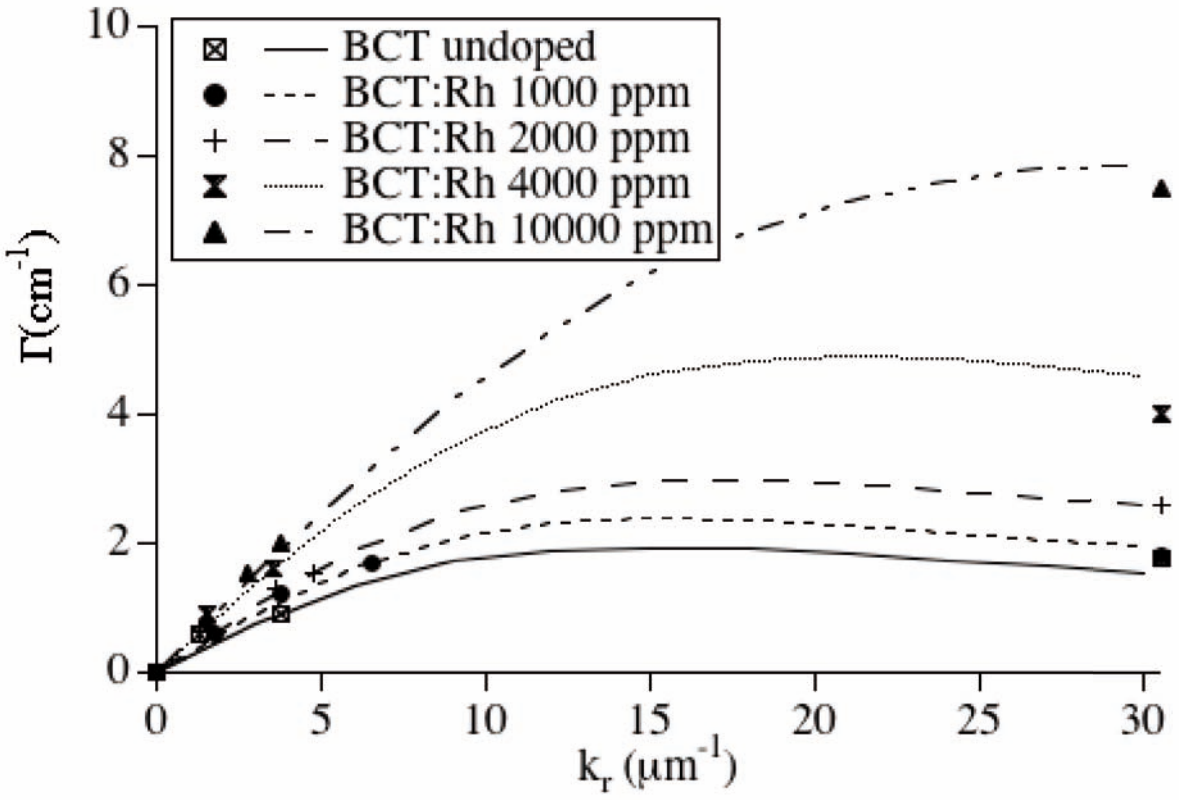

Figure 11 : Roosen et al.